Quantifying the contribution of the Megha-Tropiques mission to the estimation of daily accumulated rainfall in the Tropics

Rémy Roca, Nicolas Taburet, Estelle Lorant, Philippe Chambon, Matias Alcoba, Hélène Brogniez, Sophie Cloché, Christophe Dufour, Marielle Gosset, Clément Guilloteau

Received: 14 June 2017 | Revised: 15 March 2018 | Accepted: 3 May 2018

DOI: 10.1002/qj.3327

Quarterly Journal of the Royal Meteorological Society RMetS

Quantifying the contribution of the Megha-Tropiques mission to the estimation of daily accumulated rainfall in the Tropics

Rémy Roca[1] | Nicolas Taburet[1,*] | Estelle Lorant[2] | Philippe Chambon[3] | Matias Alcoba[4] | Hélène Brogniez[5] | Sophie Cloché[2] | Christophe Dufour[5] | Marielle Gosset[4] | Clément Guilloteau[1,4,†]

[1]Laboratoire d'Études en Géophysique et Océanographie Spatiales, Toulouse, France
[2]Institut Pierre Simon Laplace, Palaiseau, France
[3]CNRM UMR 3589, Météo-France and CNRS, Toulouse, France
[4]Géoscience Environnement Toulouse, Toulouse, France
[5]LATMOS/IPSL, UVSQ Université Paris-Saclay, UPMC University, Guyancourt, France

Correspondence
Rémy Roca, Observatoire Midi-Pyrénées, Laboratoire d'Études Géophysiques et d'Océanographie Spatiale, 14 Av. Edouard Belin, 31000 Toulouse, France.
Email: remy.roca@legos.obs-mip.fr

[*]Now with CLS.
Now with UC Irvine.

Funding information
CNRS.

Satellite estimation of accumulated precipitation is an important facet of the study of the tropical water cycle. An advanced data merging approach using infrared geostationary imagery and microwave constellation based instantaneous rain rate estimates has been implemented in the framework of the Megha-Tropiques and Global Precipitation Measurements missions. The Tropical Amount of Rainfall with Estimation of ERors (TAPEER) algorithm has been tailored to account for the loss of the MADRAS conical scanning radiometer by using the SAPHIR sounder rainfall detection capability, thanks to a novel two-constellation implementation of the algorithm. A new bias correction module based on the TRMM PR observations is also presented. The performances of this new version of the product are reviewed with emphasis on West Africa. In particular, using data-denial experiments, the contribution of SAPHIR data to the rainfall daily accumulation is quantified for various configurations of the microwave constellation and various algorithmic parameter selections. The results show that the daily accumulation statistics are well improved when SAPHIR is taken into the constellation. The improvements can be quantified using bulk statistics but are more evident following a frequency analysis. The pattern of the impact is a complex convolution of rainfall occurrence and of the Megha-Tropiques mission original sampling. Over the 20°N–20°S belt, in zonal mean, the inclusion of SAPHIR data alters the daily accumulation substantially (more than 50% of the daily accumulation) more than 10% of the time and more than 20% when conditioned upon rainfall. Under both metrics, the improvement is majored in the 12°–17° latitude band where the Megha-Tropiques mission sampling is at its maximum.

KEYWORDS
global precipitation mission constellation, satellite estimate of precipitation, tropical water and energy budget

1 | INTRODUCTION

Rainfall is at the heart of the energy cycle of the planet. Not only is rainfall part of the positive water vapour feedback loop (Stephens and Ellis, 2008) but its distribution including extremes, both in space and in intensity is anticipated to evolve in the course of climate change (Roca *et al.,* 2010a; O'Gorman *et al.,* 2012). In particular, recent theoretical considerations suggest a substantial increase in rainfall accumulation per event with global warming, with strong societal implications (Neelin *et al.,* 2017). Accumulation estimates are also identified as a key to climate model evaluation (Tapiador *et al.,* 2017). As a consequence, the monitoring of the surface rainfall distribution and accumulation has received

considerable attention over the past decades. In the Tropics where the conventional observing network is sparse, satellite observations are the only way to address this critical need for a better documentation of rainfall. Significant progress has been achieved on this front from the early attempt in the 1970s to the most recent algorithms (Kidd and Levizzani, 2011). Beyond instantaneous estimates of the surface precipitation from passive and active microwave sensors, the sampling of the atmosphere by the microwave satellite fleet has long been recognized as a key element of rainfall accumulation estimation from space.

Hence, a number of space missions and constellation concepts dedicated to the enhancement of the measurement sampling have been proposed and/or realized: the precessing Tropical Rainfall Measuring Mission (TRMM: Kummerow *et al.,* 1998) and the Megha-Tropiques (Desbois *et al.,* 2007; Roca *et al.,* 2015) missions; FLORAD (Marzano *et al.,* 2009), the Global Precipitation Measurement Mission constellation (Hou *et al.,* 2014) and more recently the Time-Resolved Observations of Precipitation structure and storm Intensity with a Constellation of Smallsats (TROPICS: Blackwell *et al.,* 2018, this issue). Along with the increased availability of the platforms came a suite of algorithms and high-level products that take benefit from these large datasets (also using geostationary infrared imagery) to provide surface rainfall accumulation estimates at various scales over the globe (or a significant part of it). The exhaustive list of products can be found on the International Precipitation Working Group (IPWG) website and we highlight here only a few that showcase the various approaches followed to use the microwave constellation observations. The TRMM Multiple Platform Algorithm (Huffman *et al.*, 2007) maps the microwave-derived instantaneous rain rate data on a regular grid and fills the gaps using infrared (IR) images. The National Oceanic and Atmospheric Administration (NOAA) Climate Precipitation Center MORPHing technique (CMORPH: Xie *et al.,* 2017) and Global Satellite Mapping of Precipitation (GSMAP: Kubota *et al.,* 2007) products both fill the gaps by morphing the Level-2 data using cloud motion winds derived from IR imagery. The Tropical Amount of Precipitation with Estimation of Errors (TAPEER) product is based on the Universally Adjusted Geostationary Operational Environmental Satellite (GOES) Precipitation Index (Xu *et al.,* 1999) and the adapted rain detection threshold and mean conditional rain rate are derived from the constellation Level-2 data to train the IR imagery (Chambon *et al.,* 2013).

Evaluation of such products at various scales over the Tropics (e.g. Hong *et al.,* 2007; Sapiano and Arkin, 2009; Roca *et al.,* 2010a; Jobard *et al.,* 2011; Gosset *et al.,* 2013; Gebremichael *et al.*, 2014; Guilloteau *et al.,* 2016; Maggioni *et al.*, 2016; Gosset *et al.,* 2018) have revealed high performances of the merged IR–microwave recent products. While these bulk statistics are useful to showcase the usefulness and the maturity of the products, they do not provide insights into the reasons for success or failure. The performance of these products not only depends upon the quality of the Level-2 retrievals but also to a large extent on the configuration of the constellation and associated sampling (Chambon *et al.,* 2012a). One objective of this article is to quantify such dependency with emphasis on the contribution of the Megha-Tropiques mission to the performance of the daily accumulated rainfall TAPEER products.

Due to the early loss of the MADRAS instrument on Megha-Tropiques (hereafter MT), the multiplatform approach that can benefit from the sampling of this low inclination mission has to rely on the Sondeur Atmosphérique du Profil Humidité Intertropicale par Radiométrie (SAPHIR) 183 GHz sounder instead of the conical scanning imager. The secondary objective of this article is hence to introduce the approach followed to include SAPHIR in the current TAPEER algorithm and to provide a description of some recent upgrades to the original implementation (Chambon *et al.,* 2013), namely a new bias correction scheme based on the TRMM Precipitation Radar (PR) data. The article is organized as follows. The data used in the study are first introduced. Then Section 3 details the functioning of the algorithm and the performances of the baseline implementation. Section 4 quantifies the contribution of the MT mission to the quality of the daily rainfall estimation. A conclusion section ends the article.

2 | DATA

2.1 | The Global Precipitation Mission constellation during boreal summer 2012

2.1.1 | Level-1 data

The characteristics of the numerous microwave-imaging platforms that were operating during 2012 boreal summer are summarized in Table 1. The GPM constellation is composed of satellites operated by meteorological, military and research space agencies (Hou *et al.,* 2014). Note that here the nominal calibration of the data is used and the benefit of the intercalibrated radiances effort of the Global Precipitation Mission (GPM) X-CAL group (Berg *et al.,* 2016) will only be used in a future version of the TAPEER product.

2.1.2 | Level-2 data

The Level-2 data correspond to the instantaneous rain rate estimates for each footprint of the microwave imagers. In this study, these rain rates are obtained using the Bayesian Rain Algorithm Including Neural network (BRAIN) algorithm that is described in detail in Viltard *et al.* (2006) and Kirstetter *et al.* (2013b). It is a fork of the original Goddard Profiling algorithm (GPROF) retrieval (Kummerow *et al.,* 1998) that follows the Bayesian framework and relies upon a database built mainly out of the TRMM PR data (see Section 2.4) and mesoscale cloud simulations. The algorithm outputs a large amount of information from the original vectors of microwave

TABLE 1 Microwave imagers and sounders on board precessing missions

Precessing		
Instrument	TMI	SAPHIR
Satellite platform	TRMM	Megha-Tropiques
Inclination (°)	35	20
Altitude (km)	402.5	867
Orbital period (mn)	92.4	100
Swath width (km)	878	1,700
Scan	Conical	Across
Channels used	10VH, 19VH, 21 V, 37VH, 85VH	183 GHZ ± 0.2; ±1.1; ±2.8; ±4.2; ±6.6; ±11.0
Typical resolution (km)	85 GHz : 8 × 6	10 (at nadir)

brightness temperatures, but in the following, only the estimated surface rain rates are used. While over the oceans all the channels from the conical imagers are used, over land the retrieval is restricted to the 37 and 85 GHz channels to minimize the surface emissivity issues with the low-frequency channels. Prior to the estimation of rain rate, a screening step is applied based on Adler *et al.* (1994) as summarized in Kacimi *et al.* (2013). Despite the various resolutions of the constellation instruments, the output resolution is set to a circular pixel of 12 km diameter (Roca *et al.,* 2015).

The BRAIN-derived Level 2 have been evaluated as part of the Megha-Tropiques Ground Validation activities (MTGV), by comparing them with ground data over the validation super-sites and at the global scale by comparing them with the TRMM PR. More details on BRAIN evaluation can be found in Gosset *et al.* (2018). One of the outcomes from BRAIN evaluation is that BRAIN exhibits strong biases, both in the detection and in the estimation of the rain rates. These biases vary a lot among regions, according to the rainfall type (with an overestimation of the amount of convective rain, and a global under-detection of small rain rates) and depending on the satellite platform used. Quantifying the propagation of these platform and rainfall regime dependent biases into the Level-4 TAPEER is complex (Chambon *et al.*, 2013), as some of the errors may compensate within the TAPEER training window.

Figure 1 illustrates the regional and rainfall regime dependence of BRAIN's biases. Here BRAIN is compared to the TRMM PR rain rates (2A25 v7) on the basis of coincident overpasses (with a time window tolerance of ±10 min), for the period June to September 2012. The PR data are aggregated to match BRAIN pixel resolution. The analysis is decomposed over several spatial windows for illustrative purposes: one window is representative of continental India (longitude 76 to 79°E; latitude 10 to 18°N; label "India"), one is representative of the Atlantic Ocean (longitude 50°W to 20°W; latitude 8 to 18°N; label "Atlan"), and two sub-windows cover the Sudanese climate regime (longitude 10°E to 10°W; latitude 8 to 10.5°N; labeled "Benin") and the Sahelian (longitude 10°E to 10°W; latitude 12 to 14.5°N; label "Sahel") regime in West Africa. Over these coincident pixels, BRAIN and PR are compared in terms of the number of pixels (at BRAIN's resolution) above a given rain rate threshold and in terms of the rainfall accumulation, also above the given threshold (i.e. for each dataset, the sum of the pixels above threshold multiplied by the rain rate on pixel is calculated). Figure 1a displays the relative bias in BRAIN, compared to PR, on the total rainfall amount. The calculations are made on coincident BRAIN–PR pixels where the BRAIN rain rate was above the threshold indicated on the *x*-axis. Figure 1b illustrates the relative bias in number of pixels detected, for each rainfall threshold. The rainfall rate (and thus rainfall type) dependence of BRAIN performance is clearly seen. BRAIN underestimates the number of rainy pixels except for relatively high threshold. The underestimation of low rain rates is somehow compensated by an overestimation of the number of pixels and of the rainfall amount for higher rain rates thresholds. The rain rate threshold for which the bias is cancelled depends strongly on the region (and to a lesser extent on the period – not shown).

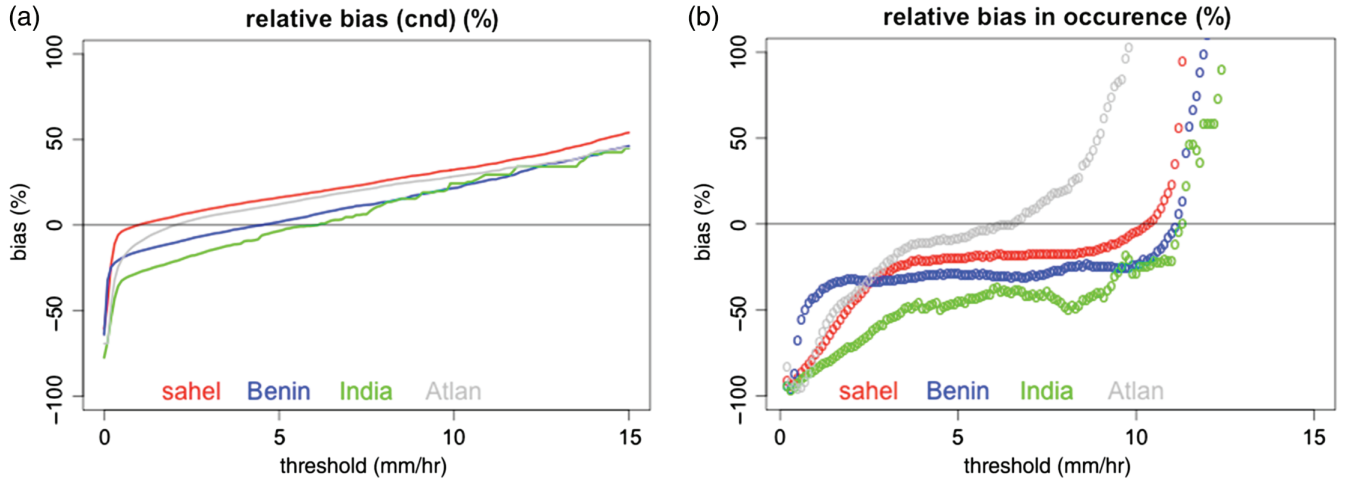

FIGURE 1 Relative bias in the Level-2 data by comparison with TRMM/precipitation radar surface rain rate, as function of rain rate threshold (see text). (a) Relative bias in rainfall amount above given threshold, conditioned on BRAIN rain rates, (b) bias (unconditional) in number of pixels above given threshold

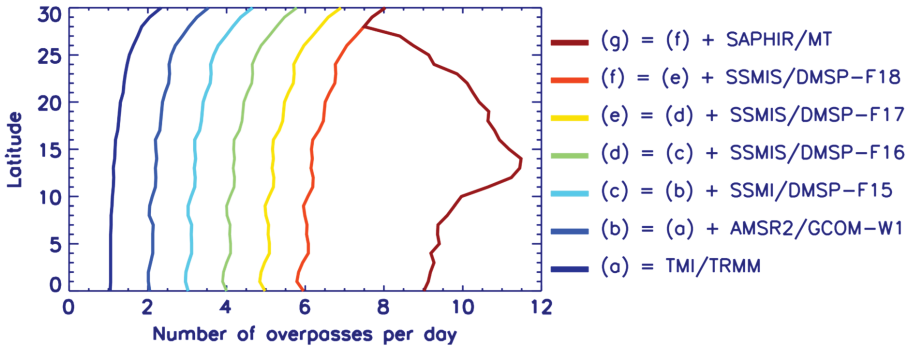

FIGURE 2 Zonal mean sampling of the GPM constellation for summer 2012

Globally biases are strongly negative in India, positive or negative depending on the sub-region in Africa, and smaller (closer to the 0 line) in the Atlantic window. The overall bias induced on TAPEER is region-dependent and a solution to correct it, based on PR climatology, was implemented as described in Section 3.3.

2.2 | The Megha-Tropiques mission and the SAPHIR data

The MT mission is described at length in various references (Desbois *et al.,* 2007; Roca *et al.,* 2010b; 2015) and here only its salient features are briefly recalled. The mission is jointly built by the Indian Space Research Organization (ISRO) and Centre National d'Études Spatiales (CNES) and was launched on 12 October 2011 from Sri Haricota in India on a unique orbit with a 20° inclination to the Equator to enhance the sampling of the tropical regions (Capderou, 2009). The platform carries on board a broad-band radiometer, Scanner for Radiation Budget (ScaRaB), dedicated to the Earth radiation budget measurements, a multichannel conically scanning microwave radiometer Microwave Analysis and Detection of Rain and Atmospheric Structure (MADRAS) that stopped operation in January 2013 after more than a year of data acquisition. The fully functional SAPHIR sounder completes the payload of the mission (Roca *et al.,* 2015). SAPHIR is a cross-track microwave sounder with six channels around 183 GHz with pixel diameter of 10 km at nadir. It is dedicated to the water vapour measurements in non-precipitating conditions (Brogniez *et al.,* 2015; Sivira *et al.,* 2015) and to assimilation efforts (Chambon *et al.,* 2015). The rainy pixels are screened thanks to a three-channel threshold approach initially introduced for intense rainfall detection (Hong *et al.,* 2005; Brogniez *et al.,* 2015; Guerbette *et al.,* 2016). This SAPHIR-derived rain mask is used in the multi-platform rainfall estimation algorithm as detailed in the next section. The weak inclination on the Equator and the elevated altitude confers a large swath to the instrument and a significant sampling contribution to the 2012 microwave imager constellation as shown in Figure 2. The 2012 configuration yields between 6 and 7 overpasses per day over the tropical belt and is augmented substantially when SAPHIR observations are accounted for, with a maximum of ∼11 overpasses per day within the 10–15° band typical of the Megha-Tropiques orbit and SAPHIR characteristics (Roca *et al.,* 2015).

2.3 | Geostationary thermal infrared data

2.3.1 | Platforms

Table 2 summarizes the details of the geostationary thermal infrared observations used to compute the accumulated precipitation and associated uncertainty for the boreal summers of 2012, 2013 and 2014. No specific effort to inter-calibrate the georing IR imagery or to correct for slight spectral differences among the sensors is undertaken. The very nature of the adaptive threshold estimation (see the section on the algorithm) as well as the overall good performance of the fleet does indeed not require such a step in dealing with the data. The TAPEER seasonal statistics exhibit no platform dependencies unlike other similar products (Roca *et al.,* 2015).

2.3.2 | Quality control

All of the input data have undergone a careful quality-control effort following the method of Szantai *et al.* (2011). A conservative approach is followed here and only images with a 100% good scan line index over the 30°S–30°N belt have been kept in the computations. Despite such a strong criterion being imposed, Table 3 further reveals that the fleet of operational geostationary imagers provides a very good coverage of the Tropics. Indeed only a few per cent of the images are missing or are not fitting our high quality standards. The major reason for low-quality data is the satellite eclipse that prevents nominal quality data acquisition. This phenomenon is mainly felt during the boreal summer June–September period on the Meteosat-7 platform and the Multi-functional Transport Satellite (MTSAT) platform. The second reason concerns the specific operation of GOES-East that prevents some of the full disk acquisition during dedicated scanning modes. The final and relatively very small contribution to low quality or missing images is the daily operation of the satellites that yields a few bad images per season.

TABLE 2 Microwave imagers on board Sun-synchronous missions

Sun-synchronous					
Instrument	AMSR-2	SSM/I	SSMIS		
Satellite platform	GCOM-W1	DMSP F15	DMSP F16	DMSP F17	DMSP F18
Equator crossing time	1:30 PM ascending	~3:45 PM ascending*	~5:45 PM ascending*	~5:45 PM ascending*	~8:15 PM ascending*
Altitude (km)	700	851	833	833	833
Swath width (km)	1,450	1,500	1,700	1,700	1,700
Scan	Conical	Conical	Conical	Conical	Conical
Channels used	10VH, 19VH, 23VH, 37VH, 89VH	19 VH, 22 V, 37VH, 85VH	19 VH, 22 V, 37VH, 91 VH	19 VH, 22 V, 37VH, 91 VH	19 VH, 22 V, 37VH, 91 VH
Typical resolution (km)	89 GHz: 5 × 3	85 GHz: 15 × 13	91 GHz: 13 × 14	91 GHz: 13 × 14	91 GHz: 13 × 14

*For the DMSP satellites, the orbits are drifting in time and the reported Equator crossing time is at their approximate summer 2012 value.

TABLE 3 Geostationary data for summer 2012, 2013 and 2014. Source WMO/OSCAR. The GOES-W and –E statistics correspond to Northern Hemisphere data acquisition. Southern Hemisphere observations details have not been reported here for sake of simplicity

			MSG				
Nominal configuration	**GOES-W**	**GOES-E**	**2012**	**2013**	**2014**	**MFG**	**MTSAT**
Satellite	**GOES-15**	**GOES-13**	**MSG-2**	**MSG-3**	**MSG-3**	**METEOSAT-7**	**MTSAT-2**
IR channel (μm)	10.2–11.2			9.80–11.8		10.5–12.5	10.3–11.3
Nadir location	135°W	75°W	0°E			57.5°E	145°E
Time resolution (min)	30	30		15		30	30
Space resolution at nadir (km)	4	4		3		5	4
Effective longitude span	175°W– 105°W	105°W –40°W		40°W– 40°E		40°E –100°E	100°E – 175°W
Missing images (%)	9.41	14.21		0.18		5.24	1.80
Low quality images (%)	2.09	2.13		0.28		0.55	0.97
Overall availability (%)	88.50	83.66		99.54		94.21	97.23

2.4 | The Tropical Rainfall Measuring Mission Precipitation Radar Level-2 products

The TRMM PR 2A25 product (Iguchi *et al.,* 2000) Version 7 is used in this study. Near-surface rain rates estimated from the TRMM PR from the common period of existence of both Megha-Tropiques and the TRMM PR (October 2011–September 2014) are used for the bias correction scheme of the TAPEER product. The Version 7 has benefited from a large investment from the developers yielding a much improved analysis (Kirstetter *et al.*, 2013a; Hamada and Takayabu, 2014). The near-surface rain rates have been further increased by 6% to account for the orbit boost, following Wang *et al.* (2014).

2.5 | West Africa ground validation data

The short assessment of the contribution of Megha-Tropiques to the constellation-based rainfall daily accumulation is performed over the MT validation super-site in Ouagadougou, Burkina Faso in West Africa (Gosset *et al.,* 2013) and using the dense research network of the African Monsoon Multidisciplinary Analysis (AMMA) – Couplage de l'Atmosphère Tropicale et Cycle Hydrologique (CATCH) programme over Niamey, Niger and over the Ouémé basin, Bénin (Lebel *et al.,* 2009). These networks have been extensively used for validation purpose (Roca *et al.,* 2010a; Gosset *et al.,* 2013; Guilloteau *et al.,* 2016) and are presented in detail in these various previous works. During summer 2012, each degree square was populated with between 15 and 41 rain-gauges insuring a well characterized estimation of the daily accumulation and a small kriging variance here used as the uncertainty of the ground-based measurements (Roca *et al.,* 2010a). These three sites correspond to different rain regimes both in terms of seasonal mean amount and in terms of the phenomenology of the associated storms and span a wide variety of cases well suited for algorithms evaluation (Gosset *et al.,* 2018, this issue).

3 | THE TROPICAL AMOUNT OF RAIN WITH ESTIMATION OF ERRORS ALGORITHM

3.1 | Algorithm description

The Tropical Amount of Rain with Estimation of Errors (TAPEER) algorithm provides both the daily accumulated rainfall as well as the associated uncertainty for each 1°×1° grid box over the whole intertropical belt. The accumulation

computation simply reads

$$Acc = \overline{R_{\text{cond}}} \times Frac \times L, \quad (1)$$

where L is the duration over which the accumulation is computed (in h), Acc stands for Accumulated rainfall amount (in mm/day), R_{cond} is the conditional rain rate (in mm/h) and $Frac$ the precipitation fraction (in %). Note that in the case of the present product, L is 24 h.

It is based on the Universally Adjusted GOES Precipitation Index technique (Xu *et al.,* 1999; Kidd *et al.,* 2003). During the first step of the algorithm called the training phase, the average of R_{cond} is computed from all the Level-2 data derived from the passive instruments available within a dedicated training volume (space+time) named $V_{R\text{cond}}$. Here $V_{R\text{cond}}$ is taken as a region of 5°×5° during 5 days, hereafter noted 5°×5°×5 day. The fraction of precipitating pixels as indicated by the Level-2 data is computed over another training volume V_{frac} which is used to derive the IR brightness temperature threshold that matches this precipitating fraction in the collocated Level-2 data and IR brightness temperature dataset. In a second step, the application phase, the actual precipitation fraction for the 1°×1°×1 day grid box is calculated thanks to the infrared threshold determined in the training phase and applied to all the infrared imagery of the day at full resolution.

The uncertainty estimate comes in the form of a standard error and reads

$$\sigma_{Acc} = \frac{\sigma}{\sqrt{N_{\text{ind}}}}, \quad (2)$$

where σ is the standard deviation in mm/day. N_{ind} is the number of independent points and is obtained thanks to variogram computations (Roca *et al.,* 2010a). The standard deviation and N_{ind} are estimated for each 1°×1°×1 day grid box and the variogram parameters are computed every 10 days over a 5°×5° region surrounding the grid box (Chambon *et al.*, 2012b). The Algorithm Theoretical Basis Document (Chambon *et al.,* 2012b) summarizes the details of the implementation of the technique and we here focus on the recent additions to this initial configuration.

Note that owing to the difficulties in the Level-2 data to retrieve realistic rain amounts in high mountainous terrains (Sohn *et al.,* 2010; Shige and Kummerow, 2016; You *et al.*, 2016), 1°×1° grid boxes with average elevation above 3,000 m are not considered in the final product and are flagged as missing. This impacts the Himalayas and the Andes regions.

3.2 | A two-constellations implementation

The accuracy of the final product is sensitive to the approach used to identify the IR threshold for rain/no rain classification and the computation of the conditional rain rate. The difficulty lies in finding a threshold that is representative of the local situation in space and time and at the same time populated with enough Level-2 data to insure statistics stability (Kummerow and Giglio, 1995). This fundamental trade-off has been explored from the GOES Precipitation Index (GPI) era (IR threshold = 235 K and R_{cond} = 3 mm/h) to the locally adjusted perspective like the one used in the TAPEER algorithm (Kidd *et al.,* 2003; Chambon *et al.*, 2012a). At the 1°×1°×1 day scale, the IR threshold for rain detection varies significantly from day to day due to the very indirect relationship between cloud top and precipitation (Kidd, 2001), and its optimum identification requires the smallest training volume to benefit from the microwave-based detection capability of the low Earth-orbiting satellites. As far as the conditional rain rates are concerned, we rely on Level-2 data that originate from a Bayesian retrieval. By consequence, the more observations used to compute R_{cond}, the closer to the reference database the estimates are. This calls for an extended training volume for conditional rain rate computations.

The analysis of the day-to-day variability of R_{cond} and of the rain fraction over the AMMA-CATCH regions during the monsoon season reveals the stability of the former (sigma ∼15%) and the strong variance of the latter (sigma ∼150%). Assuming a constant value of R_{cond} over the season only decreases the correlation coefficient of the satellite estimate with the ground data from 0.9 to 0.86. Similar statistics holds for the Burkina Faso and Bénin networks. This is consistent with multi-scale investigations performed on ground-based radar observations that at 1°×1°×1 day scale, the precipitation fraction controls the daily accumulation (Guilloteau *et al.,* 2016).

Tropics-wide analysis confirms the low variance of R_{cond} over a season compared to that of the rain fraction (Figures 3 and 4). This is indicative of the fact that at the 1°×1°×1 day scale, the accumulated rainfall day-to-day variability in the Tropics is primarily due to the detection capability of the observing system and that the conditional rain rate and the rain fraction operate on two different time-scales. A direct consequence of this analysis is that two sets of refresh time and representativity trade-offs, one for conditional rain rate and one for detection, can be elaborated upon. In particular, the computation of R_{cond} can be performed on a larger time-scale than that of the rain fraction without sacrificing too much on the accuracy of the product.

An indirect consequence is that one can use different suites of instruments to compute each of these two terms. In particular, the use of microwave sounders for the detection step permits us to increase the detection-relevant sampling and hence to use a smaller and more representative training volume (see next section for a quantitative discussion). While such an approach opens the door for using the full fleet of microwave sounders in complement to the microwave imagers fleet, it is here restricted to the single use of SAPHIR as a first prototype of such a double constellation based merging technique with emphasis on the tropical regions. The baseline followed here is to consider a training volume for R_{cond} of 5°× 5°×5 day, and of 3°×3°×1 day for the detection. The sensitivity to these assumptions is discussed in the Performances section.

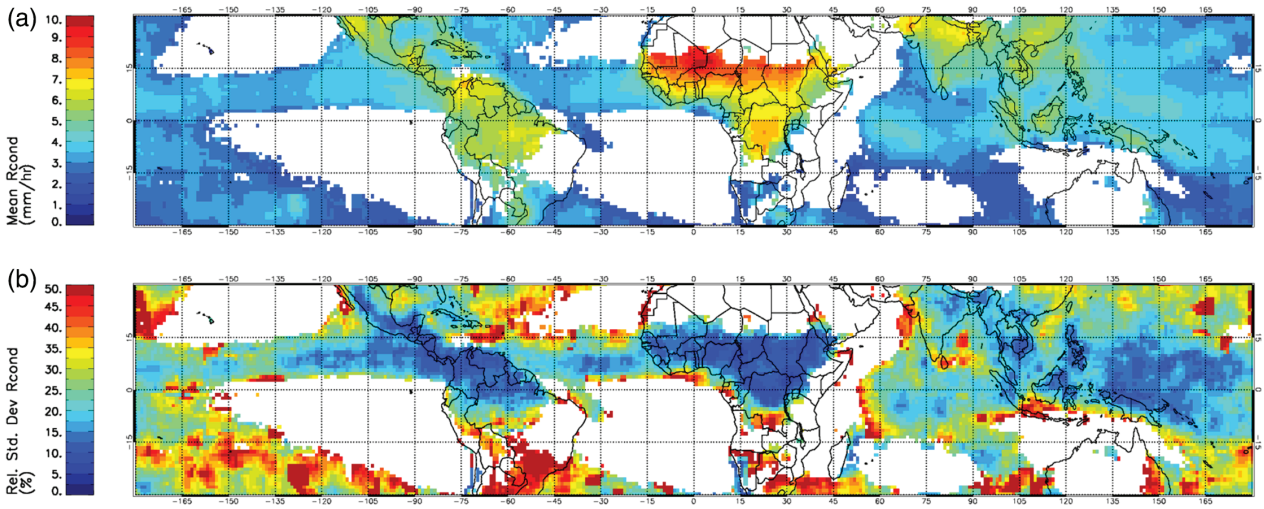

FIGURE 3 The conditional rain rate: (a) seasonal average (mm/h), (b) seasonal relative standard deviation (%)

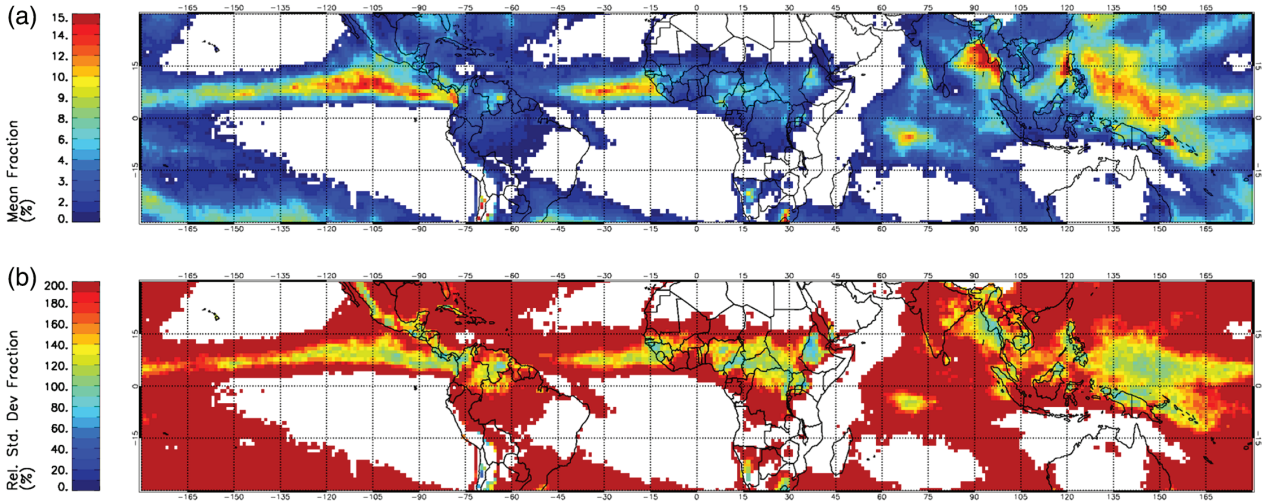

FIGURE 4 The fraction of rain: (a) seasonal average (%), (b) seasonal relative standard deviation (%)

3.3 | Bias correction scheme

3.3.1 | Rationale

The inherent limitations of the instantaneous rainfall detection and estimation issues (Elsaesser and Kummerow, 2015) propagate into the daily accumulated rainfall estimation (Chambon *et al.,* 2012b) yielding to significant global and regional bias at the monthly and seasonal scales with respect to various references (Gosset *et al.,* 2018). To cope with bias issue, various scalings of the satellite data on various references have been implemented in the literature and two major proposals have been followed. At the local scale, the use of rain-gauge data at a monthly time-scale has shown promising results over land (e.g. Huffman *et al.*, 2007; Bergès *et al.,* 2010). Some of these adjustments can also involve rain-gauges but with a climatological perspective (Huffman *et al.,* 2015). Here the latter approach is followed using large-scale regions and long-term periods to compute the bias correction. The TRMM PR products are used as a reference as a way to (a) provide correction over the oceans, (b) provide an independent estimate from the Global Precipitation Climatology Centre (GPCC) references (Becker *et al.,* 2013) and (c) to keep the final product as a satellite-only product.

3.3.2 | Details

The adjustment consists of a ratio between mean TAPEER rainfall estimates and the mean PR rain rates, where computations have been elaborated heuristically thanks to numerous attempts to account for trade-offs between statistical significance, robustness and efficiency. The proposed approach works as follows:

Averaging periods

The ratios are computed for each calendar month using a 3-month window to increase the PR and TAPEER statistics. At this stage, a 3-year period is used when TAPEER (with SAPHIR) and the TRMM Precipitation Radar overlapped to compute the statistical adjustment. It includes January–September 2012, 2013 and 2014 and October–December 2011, 2012 and 2013.

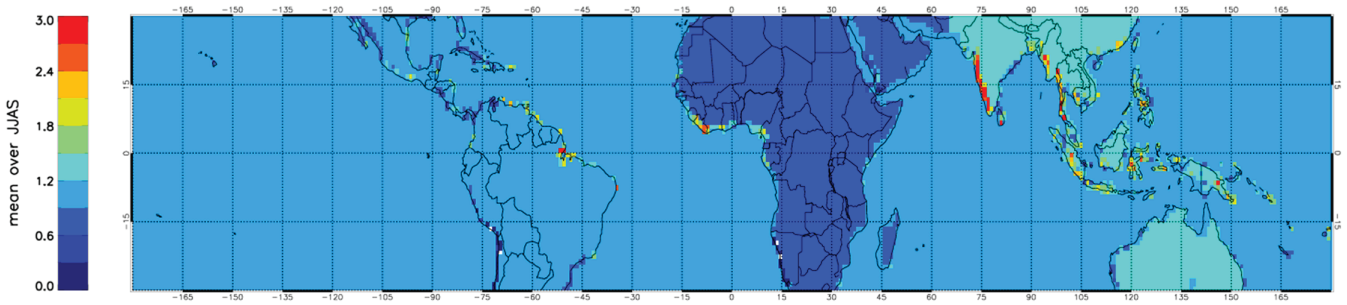

FIGURE 5 Map of the magnitude of the bias correction factor on average for JJAS 2012–2014

Land and oceanic basin

Adjustment is computed independently for land and oceanic basins to account for the Level-2 data retrievals that differ over land and ocean. The Americas, Africa and Asia continents are considered separately, as are the Atlantic and Indian Oceans. The Pacific Ocean is separated into west and east Pacific basins at the date-line. This is done in order to account for the large-scale regional variability in the TAPEER bias as revealed in the following sections.

Coastal area

In opposition to the large-scale continental land and oceanic basins, coastal regions exhibit a large geographical bias variability, principally due to the combination of the different spectral configuration for the land and oceanic retrievals. As a consequence, the statistical adjustment is here applied at the 1°×1° scale using the 1°×1° Precipitation Radar and the TAPEER totals.

3.3.3 | Magnitude of the adjustment

Figure 5 shows the distribution of the bias correction factor magnitude. Bias correction factors are greater than 1 for all continents and oceans except for Africa where it is of the order of 0.85. In all other regions, its value is of the order of 1.05–1.15, meaning that the amplitude of the correction is lower than 15%. The only exception is the Asian continent where the factor value is 1.4. Due to the local calibration, coastal bias correction factors present a larger range of values. In particular, we point out multiplicative coefficients higher than 2 in coastal west India, showing that uncalibrated TAPEER-BRAIN products present a strong rain deficit in this region. The standard deviation of the bias correction factors within a season (not shown) is of the order of a few per cent, except in coastal areas where the local calibration makes it more likely to fluctuate. These low standard deviation values indicate that our algorithm estimates do not behave differently from the climatological PR estimates along the 4-month period covered in this illustration study.

At the global scale, the impact of this bias correction increases the mean 2012 seasonal tropical daily rain amount from 2.50 to 2.87 mm/day, close to the TRMM PR 2012–2014 seasonal mean of 2.91 mm/day. The GPCP data read a little higher at 3.01 mm/day for summer 2012, probably due to their adjustments onto the GPCC data.

4 | PERFORMANCES AND SENSITIVITY STUDIES

4.1 | Data-denial experiments

The quantification of the contribution of the MT/SAPHIR observations to the GPM constellation-based rainfall estimates is performed via a series of data-denial experiments. The baseline configuration of the constellation is composed of the Level-2 data from the Sun-synchronous platforms of Table 2 plus the TMI microwave imager on board TRMM for the conditional rain estimation. The baseline configuration of the constellation for fraction estimation is the same as the baseline for conditional rain rate plus the addition of the detection of the SAPHIR on board Megha-Tropiques observations (Table 1). Then algorithm parameters are varied or the constellation members are modified to explore the sensitivity of our results to the various assumptions and to the background constellation configuration. These data-denial experiments are summarized in Table 4 and the acronyms used hereafter to refer to these experiments are introduced. Note that all the experiments have been bias-corrected using the 2012 bias departure values. These experiments are then either compared to the ground-based reference data set over West Africa and/or to the baseline results at global tropical scales. The comparisons are performed by including the uncertainty estimates when relevant. The methodology to achieve it is taken from Roca *et al.* (2010a) and it is summarized in Appendix along with the modified, uncertainty-aware, scores and metrics used.

4.2 | West Africa statistics

4.2.1 | Bulk performances and sensitivities to algorithm parameters

Table 4 summarizes the bulk statistics of the comparisons between the TAPEER products under various assumptions and the ground-based data over the three West African sites during the summer season of 2012. These performances are focused on using the errors bars of TAPEER products and

TABLE 4 The data-denial experiments

	R_{cond} estimation		Fraction estimation			
Name	**Constellation**	**Training volume**	**Constellation**	**Training volume**	**Bias correction**	**Acronym**
Reference run	Baseline Estimation	5°×5°×5 day	Baseline detection	3°×3°×1 day	Yes	Refrun
Uncorrected	Baseline Estimation	5°×5°×5 day	Baseline detection	3°×3°×1 day	No	Uncorrected
No SAPHIR	Baseline Estimation	5°×5°×5 day	Baseline detection – SAPHIR	3°×3°×1 day	Yes	NoS
Larger training	Baseline Estimation	5°×5°×5 day	Baseline detection	5°×5°×5 day	Yes	555_base
LT no SAPHIR	Baseline Estimation	5°×5°×5 day	Baseline detection – SAPHIR	5°×5°×5 day	Yes	555_NoS
1998 + SAPHIR	1998	5°×5°×5 day	1998 + SAPHIR	3°×3°×1 day	Yes	1998like+S
1998	1998	5°×5°×5 day	1998	3°×3°×1 day	Yes	1998like
No precessing	Baseline estimation-TMI	5°× 5°× 5 day	Baseline detection-TMI	3°× 3°× 1day	Yes	NoTMI -S
No TMI	Baseline estimation-TMI	5°×5°×5 day	Baseline detection-TMI-SAPHIR	3°× 3°× 1day	Yes	NoTMI+S

TABLE 5 Sensitivity to the algorithm parameters. Comparisons with ground-based references

		Cond. Ground		Cond. RMS	POD		FAR		
	R	**ave (mm/day)**	**Cond. Bias (%)**	**(mm/day)**	**Best**	**Worst**	**Best**	**Worst**	***F*-score**
Burkina									
Ref run	0.96	9.45	−18.9	2.51	0.82	0.58	0.15	0.28	1.15
Uncorrected	0.96	9.45	−11.7	2.75	0.82	0.58	0.15	0.28	1.11
NoS	0.91	9.55	−25.2	3.74	0.82	0.54	0.15	0.25	1.35
555_base	0.78	9.66	−4.0	6.11	0.78	0.56	0.15	0.31	1.41
555_NoS	0.78	9.66	−7.2	6.09	0.78	0.56	0.15	0.31	1.47
Niger									
Ref run	0.99	8.00	−6.5	1.21	0.73	0.51	0.00	0.28	0,98
Uncorrected	0.99	8.00	+1.19	1.3	0.73	0.51	0.00	0.28	0.94
NoS	0.95	8.48	−19,2	2.74	0.68	0.47	0.00	0.23	1.27
555_base	0.93	8.22	−10.1	3.39	0.72	0.42	0.05	0.25	1.34
555_NoS	0.91	8.34	−23.2	3.47	0.71	0.42	0.05	0.23	1.45
Bénin									
Ref run	0.96	9.47	−25.2	2.28	0.86	0.76	0.00	0.66	1.40
Uncorrected	0.96	9.47	−18.5	2.44	0.86	0.76	0.00	0.66	1.35
NoS	0.96	9.56	−22.5	2.00	0.86	0.76	0.00	0.66	1.35
555_base	0.80	9.91	−29.2	5.13	0.82	0.75	0.00	0.66	1.73
555_NoS	0.81	9.81	−27.8	4.78	0.82	0.75	0.00	0.66	1.69

limited to a few metrics. A companion article by Gosset *et al.* (2018 this issue) explores more systematic metrics of validation over longer periods and provides intercomparisons to complement the present compact performances assessment.

Overall, over these three sites, the reference and the uncorrected runs show very high correlations ($R > 0.96$) and very good probability of detection and false alarm rates compared to the ground-based data. The impact of the large-scale bias correction scheme is to locally increase the bias. All the statistics are made worse when SAPHIR is removed from the constellation, quantifying over these sites the importance of the Megha-Tropiques mission to the daily accumulated rainfall estimates. The data-denial experiments further indicate that the use of a larger training volume for the fraction estimate cancels the benefit of adding Megha-Tropiques to the constellation (Table 5). This degradation of the performance is even stronger in the experiment without SAPHIR (555_NoS experiment). This showcases the need to make use of the smaller training volume for better daily accumulation estimations and confirms the relevance of the selection of the training volume for our baseline configuration of the retrieval.

4.2.2 | The case-study of 4 July 2012 over Niamey

Over Niamey, 4 July 2012 stands out in the above comparison (Figure 6). Indeed without SAPHIR, the satellite estimates reads 3.5 mm (±1.7 mm), while including SAPHIR, the baseline configuration estimations yields 30.2 mm (±4.4 mm) to be compared with the rain-gauges measurement of 30.1 mm (±3.1 mm). The reasons for such a strong difference can be tracked to the IR threshold identified by the algorithm in the two configurations for this day and the actual sampling of the training volume by the SAPHIR instruments on board Megha-Tropiques. That particular day almost none of the TMI, AMRS2, SSMI or SSMIS instruments observed the

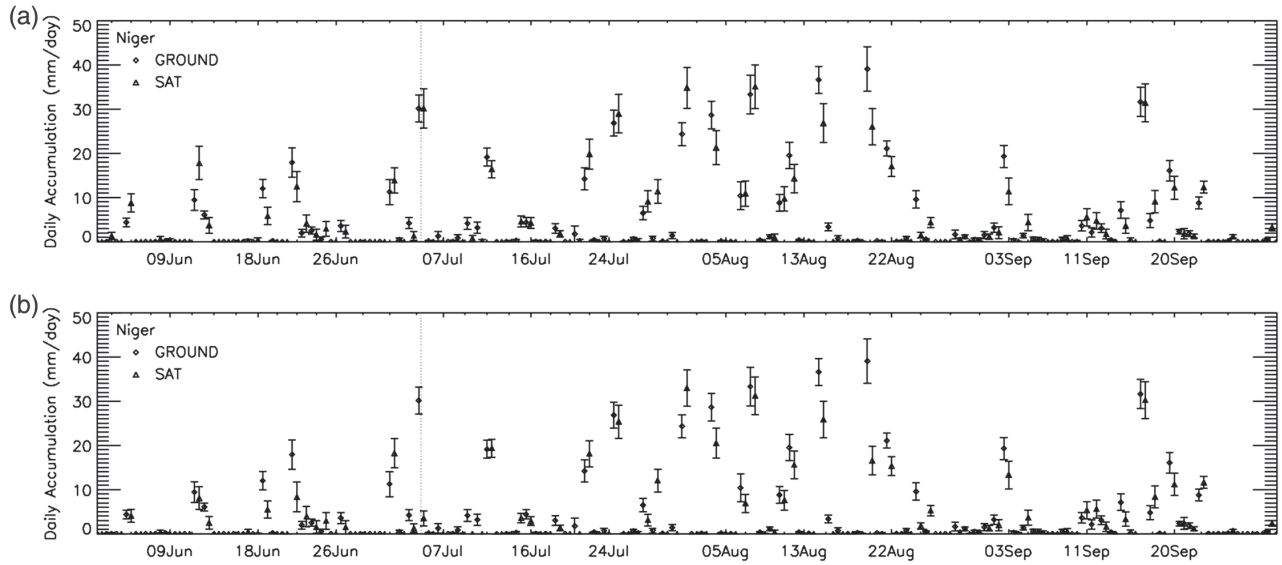

FIGURE 6 Time series over the Niger site of the satellite (triangle) and the ground-based (diamond) daily accumulation (mm/day): (a) for the baseline configuration, (b) without SAPHIR. The vertical thin dashed line indicates 4 July 2012

TABLE 6 Sensitivity to constellation configuration. Comparisons to the ground-based references

	R	Cond. Ground ave (mm/day)	Cond. Bias (%)	Cond. RMS (mm/day)	POD		FAR		*F*-score
					Best	Worst	Best	Worst	
Burkina									
98like + S	0.97	9.73	−14.4	2.54	0.79	0.57	0.15	0.31	1.15
98like	0.88	9.97	−20.8	4.88	0.79	0.52	0.15	0.25	1.42
NoTMI-S	0.91	9.77	−28.9	3.48	0.80	0.55	0.15	0.25	1.34
NoTMI+S	0.96	9.46	−18.4	2.48	0.82	0.59	0.15	0.28	1.13
Niger									
98like + S	0.99	8.09	−7.74	0.63	0.71	0.48	0.00	0.28	0.95
98like	0.92	8.8	−21.7	3.53	0.65	0.40	0.00	0.39	1.45
NoTMI-S	0.99	8.72	−11.8	1.27	0.67	0.45	0.05	0.20	1.01
NoTMI+S	0.99	8.08	−4.1	1.22	0.71	0.49	0.05	0.28	0.98
Bénin									
98like + S	0.91	9.74	−27.1	3.28	0.83	0.74	0.00	0.66	1.53
98like	0.91	9.94	−24.7	3.46	0.81	0.72	0.00	0.66	1.53
NoTMI-S	0.96	9.48	−24.7	2.16	0.86	0.76	0.00	0.66	1.38
NoTMI+S	096	9.47	−26.5	2.30	0.86	0.76	0.00	0.66	1.40

rainy structures associated with cold clouds over the Niger because they all sampled the 3°×3°×1 day sampling volume in the late morning or afternoon while the rainy event happened before 0800 UTC. The SAPHIR instrument had five overpasses over the training volume between 0000 and 0800 UTC on 4 July. As a result, SAPHIR observed 44% of the collocated pixels in the training volume corresponding to 97% of the collocated rainy pixels. The resulting IR threshold is 200.1 K for the baseline constellation but a much colder 190.4 K threshold when SAPHIR is removed, preventing the fraction estimation exceeding 1% compared to 14.8% for the baseline configuration. When the training volume is larger (5°×5°×5 day), the rainfall estimates reads 36.9 mm (±4.7 mm) with and 34.1 mm (±4.5 mm) without SAPHIR, corresponding to fractions of 18% with and 16.5% without SAPHIR, respectively. In both configurations, while the miss is not as important as in the previous case, the final estimates are less accurate than for the baseline configuration, confirming the suitability of the smaller training volume. In complement to the bulk analysis, this case-study highlights that in some cases the SAPHIR observations bring invaluable information to accurately determine the rain/no rain threshold and by consequence the daily accumulated rain estimate.

4.2.3 | Sensitivity studies to the constellation configuration

The data-denial experiments (Table 4) are further analysed to assess the sensitivity of these results to the constellation of microwave imagers, and the results are compiled in Table 6 for

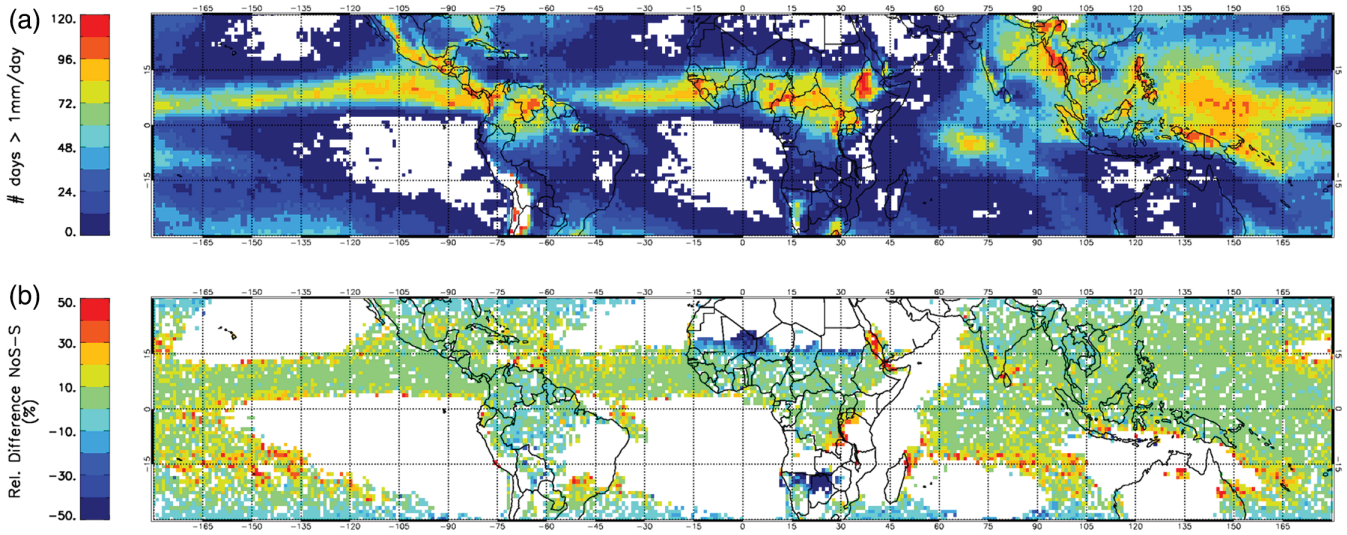

FIGURE 7 (a) Number of days with daily accumulation greater than 1 mm/day for the baseline product for the JJAS 2012 period. (b) Relative difference (%) between the NoS experiment and the baseline product. Only grid points with at least 10 days greater than 1 mm/day are represented

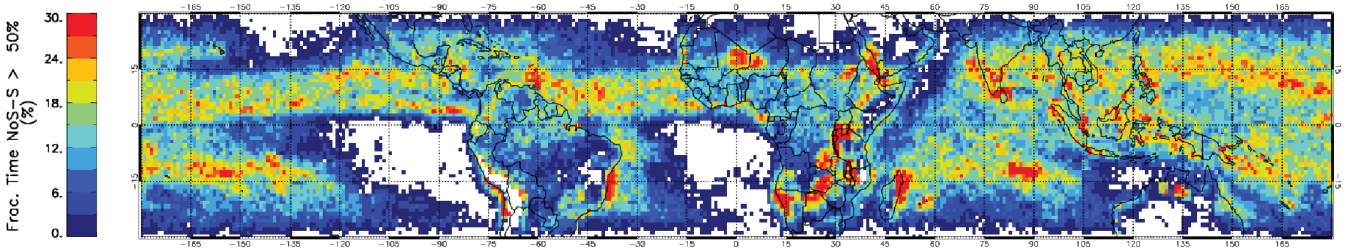

FIGURE 8 Fraction of the time for which the NoS experiment differs from the baseline product by more than 50% of the daily accumulation

the three West African sites. A 1998-like constellation and the 2012 baseline constellation without TMI are considered. First it is important to note that in both configurations the correlation, RMS and detection statistics reveal good performances of the products in the degraded cases for all the sites. In terms of bias, the Megha-Tropiques sampling clearly improves the scores except for Bénin where the impact is hardly noticeable. In both configurations and over the different rain regimes, adding the Megha-Tropiques mission improves or is neutral to the *F*-score. Comparing the results in Table 5, the No SAPHIR 2012 baseline is outperformed by the 1998-like plus SAPHIR constellation over Burkina and Niger sites, suggesting a stronger impact of Megha-Tropiques than a couple of Sun-synchronous platforms in the constellation. Over Niger and Bénin, the NoTMI-S run exhibits similar scores to the 2012 baseline run although with a slightly stronger bias over Niger (−11.8% vs. −6.5%) while such a configuration is clearly underperforming on the baseline run over Burkina with *F*-scores of 1.34 and 1.15, respectively. These local results are consistent with the Observing System Simulation Experiments and results of Chambon *et al.* (2012a) where simulated data were used to show the saturation of the performances of the constellation retrievals to the adding of Sun-synchronous observations on the top of an already dense constellation.

4.3 | Tropical-scale statistics

4.3.1 | Baseline performances

As identified over the West African networks, the bulk statistics (seasonal bias, correlation) are not substantially altered when the SAPHIR observations are removed from the 2012 constellation. When more-refined metrics are elaborated, the impact of the Megha-Tropiques data is quantified more easily. As discussed in the first part of this article, the occurrence of daily accumulation greater than 1 mm/day closely resembles the rainfall seasonal accumulation maps owing to the steadiness of R_{cond} and is likely more influenced by the enhanced detection capability brought by the Megha-Tropiques mission. Indeed, over the oceanic intertropical convergence zone (ITCZ), where more than 50 days per season read over 1 mm/day daily accumulation, the difference of the NoS experiment and the baseline products varies between 0 and 8 days, roughly within 10% of the season totals (Figure 7). Note that, even in the core of the ITCZ, some locations (white boxes in Figure 7) exhibit no sensitivity in their occurrence of rainy days to the presence of Megha-Tropiques. Over the land, similar impacts hold except for the Sahel band that reveals a stronger sensitivity with value differences ranging from −20 to −50% between the two configurations of the constellation. To complement this frequency analysis, the fraction of the time for which the NoS experiment and the baseline

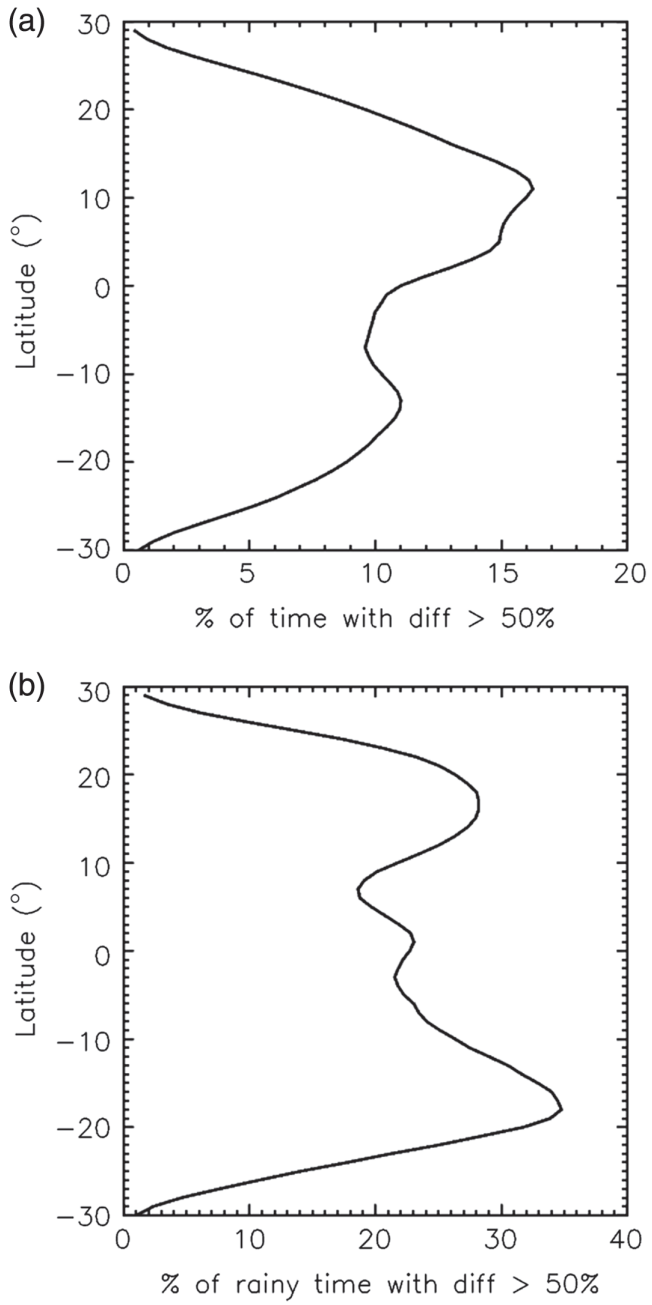

FIGURE 9 (a) Zonal mean percentage of the time for which the NoS experiment differs from the baseline product by more than 50% of the daily accumulation. (b) Zonal mean percentage of the time for which the NoS experiment differs from the baseline product by more than 50% of the daily accumulation number of days normalized by the total number of rainy days

configuration differs by more than 50% of the daily accumulations has been computed. A larger part of the intertropical belt exhibits values larger than 20%, both over the ocean and land (Figure 8). The pattern of the impact is a complex convolution of the daily rainfall accumulation patterns and the sampling patterns of the SAPHIR instrument on board the Megha-Tropiques mission.

The zonal conditional mean of these metrics indicates that over the 20°S–20°N belt more than 10% of the daily accumulation estimates are changed by more than 50% when the SAPHIR data are accounted for in the product (Figure 9a). This again results from the complex sampling pattern (Figure 2) and the rainfall distribution. When conditioned upon rainy days, the patterns further resemble the sampling patterns of Megha-Tropiques, and more than 20% of the rainy days are impacted all through the 20°S–20°N belt reaching up to 35% in the southern 15°S–17°S region where the sampling is maximized (Figure 9b).

5 | CONCLUSIONS

A new implementation of the TAPEER algorithm is introduced that provides the daily accumulated rainfall information at 1° scale over the Tropics. A climatological bias correction scheme based on the TRMM PR v7 products is presented. Two different constellations are used. One is used for estimating the mean conditional rain rates and relies on a large training volume. The second is used for the detection of the rain and the estimation of the rain fraction, and operates on a smaller training volume. In this second constellation, the detection capability of the SAPHIR sounder on board Megha-Tropiques is used. The baseline run shows very good performances when compared to a subset of ground-based data over West Africa. Thanks to a set of data-denial experiments, the impact of the Megha-Tropiques mission is quantified and the sensitivity of the products to the assumptions and parameters is assessed. Over the three West Africa sites covering different rain regimes, the impact of adding Megha-Tropiques to the constellation is neutral to positive in terms of bulk statistics. A case-study further highlights the conditions for which the MT mission brings in crucial observations that positively alter the comparison with the ground data. Tropics-wide results are computed and indicate that the MT mission, through the SAPHIR instrument, significantly alters the constellation daily accumulation estimates more than 20% of the rainy days in the zonal average. The pattern of the impact is a convolution of the rainfall occurrence and the sampling pattern of the SAPHIR instrument.

Future work is oriented towards estimating accumulated rainfall at finer time- and space scales. It is planned to make use of the GPROF Level-2 datasets (Kummerow *et al.,* 2015). In particular, recent improvements for orographic rainfall estimates (e.g. Shige and Kummerow, 2016) will likely improve the TAPEER estimate in these difficult conditions. Furthermore, it is planned to include the whole fleet of microwave sounders, and not just SAPHIR, to complement the current set of microwave imagers, thanks to recent advances in instantaneous rainfall estimates from sounders (e.g. Laviola and Levizzani, 2011; Kidd *et al.,* 2015; You *et al.,* 2016).

ACKNOWLEDGEMENTS

Numerous discussions with N. Viltard about the BRAIN algorithm are acknowledged. This study benefited from the

IPSL mesocentre ESPRI facility, which is supported by Centre national de la recherche scientifique (CNRS), UPMC, Labex L-IPSL, CNES and Ecole Polytechnique. Discussions with M. M. Dejus, CNES/MT Project manager and CNES/MT Program Manager P. Tabary are also acknowledged. This work is supported by CNRS and CNES under the Megha-Tropiques programme. The TAPEER data are available at http://www.icare.univ-lille1.fr/mt/products.

ORCID

Rémy Roca https://orcid.org/0000-0003-1843-0204
Marielle Gosset https://orcid.org/0000-0003-1064-7003
Clément Guilloteau https://orcid.org/0000-0001-8142-7740

REFERENCES

Adler, R.F., Huffman, G.J. and Keehn, P.R. (1994) Global tropical rain estimates from microwave-adjusted geosynchronous IR data. *Remote Sensing Reviews*, 11, 125–152.

Becker, A., Finger, P., Meyer-Christoffer, A., Rudolf, B., Schamm, K., Schneider, U. and Ziese, M. (2013) A description of the global land-surface precipitation data products of the Global Precipitation Climatology Centre with sample applications including centennial (trend) analysis from 1901–present. *Earth System Science Data*, 5, 71–99. https://doi.org/10.5194/essd-5-71-2013.

Berg, W., Bilanow, S., Chen, R., Datta, S., Draper, D., Ebrahimi, H., Farrar, S., Jones, W., Kroodsma, R., McKague, D., Payne, V., Wang, J., Wilheit, T. and Yang, J. (2016) Intercalibration of the GPM microwave radiometer constellation. *Journal of Atmospheric and Oceanic Technology*, 33, 2639–2654. https://doi.org/10.1175/JTECH-D-16-0100.1.

Bergès, J.C., Jobard, I., Chopin, F. and Roca, R. (2010) EPSAT-SG: a satellite method for precipitation estimation; its concepts and implementation for the AMMA experiment. *Annales de Geophysique*, 28, 289–308. https://doi.org/10.5194/angeo-28-289-2010.

Blackwell, W.J., Braun, S., Bennartz, R., Velden, C., DeMaria, M., Atlas, R., Dunion, J., Marks, F., Rogers, R., Annane, B. and Leslie, R.V. (2018) An overview of the TROPICS NASA Earth Venture mission. *Quarterly Journal of the Royal Meteorological Society*, 144, 16–26. https://doi.org/10.1002/qj.3290.

Brogniez, H., Clain, G. and Roca, R. (2015) Validation of upper tropospheric humidity from SAPHIR onboard Megha-Tropiques using tropical soundings. *Journal of Applied Meteorology and Climatology*, 54, 896–908. https://doi.org/10.1175/JAMC-D-14-0096.1.

Capderou, M. (2009) *Sampling: comparison with other meteorological satellites*, Megha-Tropiques Technical Memorandum No.1. Available at: http://meghatropiques.ipsl.polytechnique.fr/available-documents/mttm/index.html [Accessed 13 June 2017].

Chambon, P., Jobard, I., Roca, R. and Viltard, N. (2013) An investigation of the error budget of tropical rainfall accumulation derived from merged passive microwave and infrared satellite measurements. *Quarterly Journal of the Royal Meteorological Society*, 139, 879–893. https://doi.org/10.1002/qj.1907.

Chambon, P., Roca, R., Jobard, I. and Capderou, M. (2012a) The sensitivity of tropical rainfall estimation from satellite to the configuration of the microwave imagers constellation. *IEEE Geoscience and Remote Sensing Letters*, 99, 1–5. https://doi.org/10.1109/LGRS.2012.2227668.

Chambon, P., Roca, R., Jobard, I. and Aublanc, J. (2012b) *TAPEER-BRAIN PRODUCT algorithm theoretical basis document*. Megha-Tropiques Technical Memorandum No.5. Available at http://meghatropiques.ipsl.polytechnique.fr/available-documents/mttm/index.html [Accessed 13 June 2017].

Chambon, P., Meunier, L.F., Guillaume, F., Piriou, J.M., Roca, R. and Mahfouf, J.F. (2015) Investigating the impact of the water vapour sounding observations from SAPHIR on board Megha-Tropiques into the ARPEGE global model. *Quarterly Journal of the Royal Meteorological Society*, 141, 1769–1779. https://doi.org/10.1002/qj.2478.

Desbois, M., Capderou, M., Eymard, L., Roca, R., Viltard, N., Viollier, M. and Karouche, N. (2007) Megha-Tropiques: un satellite hydrométéorologique franco-indien. *La Météorologie*, 57(8), 19–27.

Elsaesser, G.S. and Kummerow, C.D. (2015) The sensitivity of rainfall estimation to error assumptions in a Bayesian passive microwave retrieval algorithm. *Journal of Applied Meteorology and Climatology*, 54, 408–422. https://doi.org/10.1175/JAMC-D-14-0105.1.

Gebremichael, M., Bitew, M.M., Hirpa, F.A. and Tesfay, G.N. (2014) Accuracy of satellite rainfall estimates in the Blue Nile Basin: lowland plain versus highland mountain. *Water Resources Research*, 50, 8775–8790.

Gosset, M., Viarre, J., Quantin, G. and Alcoba, M. (2013) Evaluation of several rainfall products used for hydrological applications over West Africa using two high-resolution gauge networks. *Quarterly Journal of the Royal Meteorological Society*, 139, 923–940.

Gosset, M., Alcoba, M., Roca, R., Cloché, S. and Urbani, G. (2018) Evaluation of TAPEER daily estimates and comparisons with other GPM-era products against high-resolution gauge networks in West Africa. *Quarterly Journal of the Royal Meteorological Society*, 144, 255–269. https://doi.org/10.1002/qj.3335.

Guerbette, J., Mahfouf, J.-F. and Plu, M. (2016) Towards the assimilation of all-sky microwave radiances from the SAPHIR humidity sounder in a limited area NWP model over tropical regions. *Tellus A*, 68(1), 28620. https://doi.org/10.3402/tellusa.v68.28620.

Guilloteau, C., Roca, R. and Gosset, M. (2016) A multiscale evaluation of the detection capabilities of high-resolution satellite precipitation products in West Africa. *Journal of Hydrometeorology*, 17, 2041–2059. https://doi.org/10.1175/JHM-D-15-0148.1.

Hamada, A. and Takayabu, Y.N. (2014) A removal filter for suspicious extreme rainfall profiles in TRMM PR 2A25 Version-7 data. *Journal of Applied Meteorology and Climatology*, 53, 1252–1271.

Hong, G., Heygster, G., Miao, J. and Kunzi, K. (2005) Detection of tropical deep convective clouds from AMSU-B water vapor channels measurements. *Journal of Geophysical Research*, 110, D05205. https://doi.org/10.1029/2004JD004949.

Hong, Y., Gochis, D., Cheng, J.T., Hsu, K.L. and Sorooshian, S. (2007) Evaluation of PERSIANN-CCS rainfall measurement using the NAME event rain gauge network. *Journal of Hydrometeorology*, 8(3), 469–482. https://doi.org/10.1175/JHM574.1.

Hou, A., Y., Kakar, R.K., Neeck, S., Azarbarzin, A.A., Kummerow, C.D., Kojima, M., Oki, R., Nakamura, K. and Iguchi, T. (2014) The global precipitation measurement mission. *Bulletin of the American Meteorological Society*, 95, 701–722. https://doi.org/10.1175/BAMS-D-13-00164.1.

Huffman, G.J., Bolvin, D.T., Nelkin, E.J., Wolff, D.B., Adler, R.F., Gu, G., Hong, Y., Bowman, K.P. and Stocker, E.F. (2007) The TRMM Multisatellite Precipitation Analysis (TMPA): Quasi-Global, Multiyear, Combined-Sensor Precipitation Estimates at Fine Scales. *Journal of Hydrometeorology*, 8, 38–55. https://doi.org/10.1175/JHM560.1.

Huffman, G.J., Bolvin, D.T. and Nelkin, E.J. (2015) Integrated Multi-Satellite Retrievals for GPM (IMERG) technical documentation. NASA Doc., 48 pp. Available online at http://pmm.nasa.gov/sites/default/files/document_files/IMERG_doc.pdf.

Iguchi, T., Kozu, T., Meneghini, R., Awaka, J. and Okamoto, K.I. (2000) Rain-profiling algorithm for the TRMM precipitation radar. *Journal of Applied Meteorology*, 39(12), 2038–2052.

Jobard, I., Chopin, F., Berges, J.C. and Roca, R. (2011) An intercomparison of 10-day satellite precipitation products during West African monsoon. *International Journal of Remote Sensing*, 32(9), 2353–2376.

Kacimi, S., Viltard, N. and Kirstetter, P.-E. (2013) A new methodology for rain identification from passive microwave data in the Tropics using neural networks. *Quarterly Journal of the Royal Meteorological Society*, 139, 912–922.

Kelly, B.C. (2007) Some aspects of measurement error in linear regression of astronomical data. *The Astrophysical Journal*, 665, 1489–1506.

Kidd, C. (2001) Satellite rainfall climatology: a review. *International Journal of Climatology*, 21(9), 1041–1066.

Kidd, C. and Levizzani, V. (2011) Status of satellite precipitation retrievals. *Hydrology and Earth System Sciences*, 15, 1109–1116.

Kidd, C., Kniveton, D.R., Todd, M.C. and Bellerby, T.J. (2003) Satellite rainfall estimation using a combined passive microwave and infrared algorithm. *Journal of Hydrometeorology*, 4, 1088–1104.

Kidd, C., Matsui, T., Chern, J., Mohr, K., Kummerow, C. and Randel, D. (2015) Precipitation estimates from cross-track passive microwave observations using a physically based retrieval scheme. *Journal of Hydrometeorology*, 17, 383–400. https://doi.org/10.1175/JHM-D-15-0051.1.

Kirstetter, P.E., Hong, Y., Gourley, J.J., Schwaller, M., Petersen, W. and Zhang, J. (2013a) Comparison of TRMM 2A25 products version 6 and version 7 with NOAA/NSSL ground radar-based National Mosaic QPE. *Journal of Hydrometeorology*, 14(2), 661–669. https://doi.org/10.1175/JHM-D-12-030.1.

Kirstetter, P.E., Viltard, N. and Gosset, M. (2013b) An error model for instantaneous satellite rainfall estimates: evaluation of BRAIN-TMI over West Africa. *Quarterly Journal of the Royal Meteorological Society*, 139, 894–911. https://doi.org/10.1002/qj.1964.

Kubota, T., Shige, S., Hashizume, H., Aonashi, K., Takahashi, N., Seto, S., Hirose, M., Takayabu, Y.N., Nakagawa, K., Iwanami, K., Ushio, T., Kachi, M. and Okamoto, K. (2007) Global precipitation map using satellite-borne microwave radiometers by the GSMaP project: production and validation. *IEEE Transactions on Geoscience and Remote Sensing*, 45(7), 2259–2275.

Kummerow, C. and Giglio, L. (1995) A method for combining passive microwave and infrared observations. *Journal of Atmospheric and Oceanic Technology*, 12, 33–45.

Kummerow, C., Barnes, W., Kozu, T., Shiue, J. and Simpson, J. (1998) The Tropical Rainfall Measuring Mission (TRMM) sensor package. *Journal of Atmospheric and Oceanic Technology*, 15, 808–816.

Kummerow, C.D., Randel, D.L., Kulie, M., Wang, N., Ferraro, R., Joseph Munchak, S. and Petkovic, V. (2015) The evolution of the Goddard profiling algorithm to a fully parametric scheme. *Journal of Atmospheric and Oceanic Technology*, 32, 2265–2280. https://doi.org/10.1175/JTECH-D-15-0039.1.

Laviola, S. and Levizzani, V. (2011) The 183-WSL fast rain rate retrieval algorithm. Part I: Retrieval design. *Atmospheric Research*, 99, 443–461.

Lebel, T., Parker, D.J., Flamant, C., Bourles, B., Marticorena, M., Mougin, E., Peugeot, C., Diedhiou, A., Haywood, J.M., Ngamini, J.B., Polcher, J., Redelsperger, J.L. and Thorncroft, C.D. (2009) The AMMA field campaigns: multiscale and multidisciplinary observations in the West African region. *Quarterly Journal of the Royal Meteorological Society*, 136(S1), 8–33.

Maggioni, V., Meyers, P.C. and Robinson, M.D. (2016) A review of merged high-resolution satellite precipitation product accuracy during the Tropical Rainfall Measuring Mission (TRMM) era. *Journal of Hydrometeorology*, 17, 1101–1117. https://doi.org/10.1175/JHM-D-15-0190.1.

Marzano, F.S., Cimini, D., Memmo, A., Montopoli, M., Rossi, T., De Sanctis, M., Lucente, M., Mortari, D. and Di Michele, S. (2009) Flower constellation of millimeter-wave radiometers for tropospheric monitoring at pseudo-geostationary scale. *IEEE Transactions on Geoscience and Remote Sensing*, 47, 3107–3122.

Neelin, J.D., Sahany, S., Stechmann, S.N. and Bernstein, D.N. (2017) Global warming precipitation accumulation increases above the current-climate cutoff scale. *PNAS 2017*, 114(6), 1258–1263. https://doi.org/10.1073/pnas.1615333114.

O'Gorman, P.A., Allan, R.P., Byrne, M.P. and Previdi, M. (2012) Energetic constraints on precipitation under climate change. *Surveys in Geophysics*, 33, 585–608. https://doi.org/10.1007/s10712-011-9159-6.

Roca, R., Chambon, P., Jobard, I., Kirstetter, P.-E., Gosset, M. and Bergès, J.C. (2010a) Comparing satellite and surface rainfall products over West Africa at meteorologically relevant scales during the AMMA campaign using error estimates. *Journal of Applied Meteorology and Climatology*, 49(4), 715–731.

Roca, R., Bergès, J.C., Brogniez, H., Capderou, M., Chambon, P., Chomette, O., Cloché, S., Fiolleau, T., Jobard, I., Lémond, J., Ly, M., Picon, L., Raberanto, P., Szantai, A. and Viollier, M. (2010b) On the water and energy cycle in the Tropics. *Comptes Rendus Geoscience*, 342(4–5), 390–402. https://doi.org/10.1016/j.crte.2010.01.003.

Roca, R., Brogniez, H., Chambon, P., Chomette, O., Cloché, S., Gosset, M., Mahfouf, J.F., Raberanto, P. and Viltard, N. (2015) The Megha-Tropiques mission: a review after three years in orbit. *Frontiers in Earth Science*, 3, 1–14. https://doi.org/10.3389/feart.2015.00017.

Shige, S. and Kummerow, C.D. (2016) Precipitation-top heights of heavy orographic rainfall in the Asian monsoon region. *Journal of the Atmospheric Sciences*, 73, 3009–3024. https://doi.org/10.1175/JAS-D-15-0271.1.

Sivira, R., Brogniez, H., Mallet, C. and Oussar, Y. (2015) A layer-averaged relative humidity profile retrieval for microwave observations: design and results for the Megha-Tropiques payload. *Atmospheric Measurement Techniques*, 8, 1055–1071. https://doi.org/10.5194/amt-8-1055-2015.

Sohn, B.J., Han, H.-J. and Seo, E.-K. (2010) Validation of satellite-based high-resolution rainfall products over the Korean peninsula using data from a dense rain gauge network. *Journal of Applied Meteorology and Climatology*, 49, 701–714.

Stephens, G.L. and Ellis, T.D. (2008) Controls of global-mean precipitation increases in global warming GCM experiments. *Journal of Climate*, 21, 6141–6155. https://doi.org/10.1175/2008JCLI2144.1.

Szantai, A., Six, B., Cloché, S. and Sèze, G. (2011) *Quality of geostationary satellite images*, Megha-Tropiques Technical Memorandum No.3. Available at: http://meghatropiques.ipsl.polytechnique.fr/available-documents/mttm/index.html [Accessed 13 June 2017].

Tapiador, F.J., Navarro, A., Levizzani, V., García-Ortega, E., Huffman, G.J., Kidd, C., Kucera, P.A., Kummerow, C.D., Masunaga, H., Petersen, W.A., Roca, R., Sánchez, J.-L., Tao, W.-K. and Turk, F.J. (2017) Global precipitation measurements for validating climate models. *Atmospheric Research*, 197, 1–20.

Viltard, N., Burlaud, C. and Kummerow, C.D. (2006) Rain retrieval from TMI brightness temperature measurements using a TRMM PR-based database. *Journal of Applied Meteorology and Climatology*, 45, 455–466.

Wang, J., Adler, R.F., Huffman, G.J. and Bolvin, D. (2014) An updated TRMM composite climatology of tropical rainfall and its validation. *Journal of Climate*, 27, 273–284. https://doi.org/10.1175/JCLI-D-13-00331.1.

Xie, P., Joyce, R., Wu, S., Yoo, S., Yarosh, Y., Sun, F. and Lin, R. (2017) Reprocessed, bias-corrected CMORPH global high-resolution precipitation estimates from 1998. *Journal of Hydrometeorology*, 18, 1617–1641 https://doi.org/10.1175/JHM-D-16-0168.1.

Xu, L., Gao, X., Sorooshian, S., Arkin, P.A. and Imam, B. (1999) A microwave infrared threshold technique to improve the GOES precipitation index. *Journal of Applied Meteorology*, 38, 569–579.

You, Y., Wang, N., Ferraro, R. and Meyers, P. (2016) A prototype precipitation retrieval algorithm over land for ATMS. *Journal of Hydrometeorology*, 17, 1601–1621 https://doi.org/10.1175/JHM-D-15-0163.1.

How to cite this article: Roca R, Taburet N, Lorant E, *et al*. Quantifying the contribution of the Megha-Tropiques mission to the estimation of daily accumulated rainfall in the Tropics. *Q J R Meteorol Soc* 2018;144 (Suppl. 1):49–63. https://doi.org/10.1002/qj.3327

APPENDIX

The strength of the TAPEER algorithm is to provide error bars on the daily rainfall estimates. This information is very valuable when comparing two datasets, as accounting for the error bars can significantly change some metrics like the correlation, root-mean-square error (RMS), bias and contingency tables as shown in Roca *et al.* (2010a). For computing correlations, biases and RMS of the regression presented in this article between the TAPEER rain estimates and rain-gauge data, accounting for their respective errors, we used the Kelly (2007) approach that is based on a maximum likelihood estimate technique.

Contingency tables can also be computed taking into account error bars. Indeed, when the relative standard error is larger than 100% of the rain estimate provided by either rain-gauges or TAPEER, this affects the rain detection statistics. One conservative way to compute a probability of

detection (POD) and a false alarm rate (FAR) accounting for errors is to choose the worst scenarios, which minimize the POD and maximize the FAR. This can be achieved by defining the POD as the ratio of the number of cases where RainSat-errorSat>0 and RainGauges>0 over the number of cases where RainGauges>0, and the FAR as the ratio of the number of cases where RainSat>0 and RainGauges-errorGauges<=0 over the number of cases where RainSat>0.

In order to compare the various experiments described in this article, another metric is used which combines the metrics described before into a single one called the F-score as defined in Chambon *et al.* (2012a). The F-score accounts for the biases, RMS, POD and FAR between the TAPEER estimates and the ground measurements, and their associated uncertainties. The bias and RMS are computed using the Kelly regression, so as to account for the error bars as indicated by the 'REG' subscript in Equation (4). It reads:

$$F = 1 + \left|\frac{BIAS_{\mathrm{REG}}}{\langle R_{\mathrm{REF}}\rangle}\right| + \left|\frac{RMS_{\mathrm{REG}}}{\langle \mathrm{R}_{\mathrm{REF}}\rangle}\right| - POD_{\mathrm{worst}} + FAR_{\mathrm{worst}}, \tag{A1}$$

where $<R_{\mathrm{REF}}>$ is the average rainfall of the ground measurements. With this metric, the lower the F-score is, the better the TAPEER estimations are.